




Polarization anomaly in high harmonics in the crossover region between perturbative and extreme nonlinearity in GaAs

Fumiya Sekiguchi ,* Go Yumoto , Hideki Hirori , and Yoshihiko Kanemitsu [†]
Institute for Chemical Research, Kyoto University, Uji, Kyoto 611-0011, Japan

 (Received 25 February 2022; revised 23 November 2022; accepted 29 November 2022; published 20 December 2022)

We investigate the characteristics of high harmonics (HHs) unique to the nonperturbative nonlinear regime. We show that the polarization state of HHs generated from GaAs changes drastically across the crossover from the weak-field perturbative regime to the strong-field extreme nonlinear regime, while the linearly polarized infrared excitation field (E_{exc}) is fixed to a particular crystal direction. The dependence on the E_{exc} -field strength reveals that multiple emission processes with different nonlinear orders and temporal phases contribute to each order HH, and the interference among them plays a pivotal role. This interference manifests itself as a unique phenomenon: a large HH ellipticity emerges in the course of crossover, despite the fact that GaAs hosts no magnetization or linear birefringence. These results demonstrate that not only the material's symmetry but also the ultrafast nonlinear dynamics largely affects the HH polarization, and hence, HH polarization and its E_{exc} -field dependence provide a useful experimental tool to probe ultrafast coherent dynamics in light-driven solid-state materials.

DOI: [10.1103/PhysRevB.106.L241201](https://doi.org/10.1103/PhysRevB.106.L241201)

I. INTRODUCTION

Responses in the direction perpendicular to the applied external field, which we refer to as “orthogonal responses (ORs),” emerge in solids under low symmetric conditions. In transport phenomena, the Hall effect appears under broken time-reversal symmetry. In optical phenomena, the Faraday/Kerr effect and birefringence appear under broken time-reversal and spatial-inversion symmetry, respectively. Besides being of fundamental interest, these effects provide useful tools to access material properties. In optics, OR affects the polarization of the light, on which information of the electronic and magnetic structure of the material is imprinted [1].

Although the characteristics of OR in relation to symmetry are established in the linear regime, they are highly nontrivial in the nonlinear regime. Indeed, a recent report on the nonlinear Hall effect without breaking time-reversal symmetry has attracted intense interest [2,3]. It is therefore promising to explore novel optical phenomena in solids, even in standard semiconductor materials, by focusing on their nonlinear OR [4]. Research on nonlinear optical phenomena in solids has made significant progress owing to recent advances in ultrafast laser technology that enables generation of intense midinfrared or terahertz pulses with a tabletop setup [5–9]. A paramount example is high harmonic generation (HHG) from solids [10–14]. Under the excitations with such intense pulses, carriers excited in a wide region in the Brillouin zone are thought to contribute to HHG with reflecting the anisotropy of the solid-state electronic structures [15,16]. Hence, HHG is expected to be an alternative tool to access the band structures [17–21], transition dipoles [22,23], valence electrons [15,24],

Berry curvatures [25–27], and the coherent carrier dynamics taking place therein.

An important property of HHs is the polarization state [28,29], which reflects not only the amplitude but also the temporal phase of nonlinear OR. Here, it should be noted that nonlinear dynamics leading to HHG requires a picture beyond the perturbative regime [11–14]. This is important because in the course of transition from the weak-field perturbative regime to the strong-field extreme nonlinear regime, the coherent carrier dynamics should change their characteristics, which can largely modify the HH properties such as polarization states. However, the term “nonperturbative” is commonly used to simply indicate that the excitation-field (E_{exc} -field) dependence of the n th HH yield deviates from the E_{exc}^{2n} power law. Other hallmarks of the nonperturbative regime reported so far are limited to the *dependence of HH yields* on the HH order or the E_{exc} -field strength, i.e., the plateau structures in the HH spectra [13,14,17,30,31] or oscillatory behavior in the E_{exc} -field dependence [32,33]. In other words, it remains elusive whether *each HH* obtains a unique property beyond the conventional perturbative regime.

In this study, we investigate HHG by linearly polarized E_{exc} across the perturbative to extreme nonlinearity (PEN) crossover in an archetypal direct-gap semiconductor GaAs. GaAs has a cubic crystal structure under time-reversal symmetry, which hosts no magnetization or linear birefringence. Nevertheless, a finite HH component perpendicular to E_{exc} , I_{\perp} , appears when E_{exc} is applied in a direction of low crystal symmetry. We found that the contribution from I_{\perp} becomes significant in the middle of the PEN crossover, inducing an anomaly in the HH polarization with a large ellipticity.

II. EXPERIMENTAL METHOD

In the experiment, HHs were generated from the (100) surface of bulk GaAs and measured with reflection geometry

*sekiguchi.fumiya.2n@kyoto-u.ac.jp

[†]kanemitsu@scl.kyoto-u.ac.jp

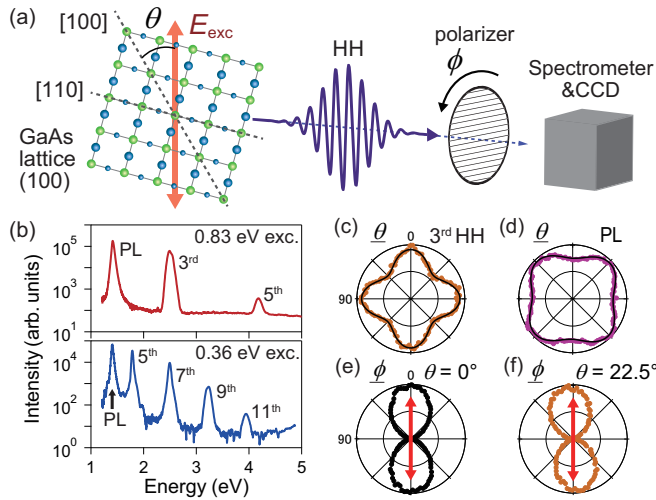


FIG. 1. (a) Schematic image of the high harmonic (HH) generation from the (100)-surface GaAs by excitation electric field E_{exc} . θ and ϕ denote the angle of the [100] crystal axis and the detection polarizer relative to E_{exc} , respectively. (b) HH spectra generated by the excitation of (upper panel) 0.83 eV, 4 MV/cm and (lower panel) 0.36 eV, 7 MV/cm. (c), (d) θ dependence of (c) 3rd HH yield and (d) PL intensity, without resolving polarization. (e), (f) Polarization state of the 3rd HH generated at (e) $\theta = 0^\circ$ and (f) $\theta = 22.5^\circ$. Arrows indicate the E_{exc} direction. For (c)–(f), $E_{\text{exc}} = 1.3$ MV/cm.

(see Supplemental Material [34]). For the excitation, we used linearly polarized infrared pulses with a photon energy of 0.83 or 0.36 eV and with a pulse duration of around 100 fs. Figure 1(a) shows a schematic picture of a GaAs (100) lattice with E_{exc} in the vertical direction. θ is the angle between E_{exc} and the crystal orientation, which was controlled by rotating the crystal. Figure 1(b) shows representative HH spectra obtained by the 0.83-eV and 0.36-eV excitation, where odd-order HHs were observed up to 5th and 11th order, respectively, lying above the photoluminescence (PL).

III. RESULTS

First, we discuss the HH properties generated by the 0.83-eV excitation, under a weak E_{exc} field of 1.3 MV/cm. Figures 1(c) and 1(d) show the crystal-orientation anisotropy, i.e., θ dependence of the 3rd HH yield and PL intensity, respectively, detected without polarization resolution. The E_{exc} -field strength lies in the perturbative region. Indeed, Fig. 1(c) is consistent with the anisotropy expected from the perturbative 3rd-harmonic generation [35]. Figure 1(d) is also consistent with two-photon absorption [36], given that the PL intensity of GaAs at room temperature is proportional to the square of the photoinjected carrier density [34]. It is noteworthy that the 3rd HH is most efficiently generated at $\theta = 0^\circ$, i.e., E_{exc} is applied along the [100] direction in which the photoinjected carrier density is at a minimum. This discrepancy of anisotropy highlights the fact that HHG is an outcome of coherent dynamics where virtual excitation processes play an essential role [37].

Figures 1(e) and 1(f) show the polarization states of the 3rd HH. The polar plots represent the HH intensity measured while rotating the polarizer before the detector. ϕ denotes

the angle between the polarizer transmission axis and E_{exc} . When $\theta = 0^\circ$, i.e., E_{exc} is along the [100] direction, the HH polarization is linear, identically to E_{exc} . This is because OR is zero, since generation of a perpendicular polarization relative to E_{exc} is forbidden due to the high symmetry (see Supplemental Material [34]). In contrast, when E_{exc} is in a direction of low symmetry, e.g., $\theta = 22.5^\circ$, a finite perpendicular polarization can be induced [Fig. 1(f)]. Thus, the HH intensity has a finite perpendicular component I_{\perp} , that induces different HH polarizations from E_{exc} . This symmetry argument holds for any E_{exc} -field strength. Figure 1(f) demonstrates that the polarization of the 3rd HH is slightly tilted by $\sim 6^\circ$ from E_{exc} , which is again consistent with the conventional perturbation theory [35]. Note that in the linear response, GaAs shows no birefringence because of the cubic crystal structure [34]. Thus, this result is a hallmark of OR emerging in the nonlinear response. However, the observed impact on the HH polarization is limited, as the ratio of the perpendicular to parallel component, $R_{\perp\parallel} = I_{\perp}/I_{\parallel}$, is only $\sim 1\%$.

The HH property changes drastically when the E_{exc} field increases and goes beyond the conventional perturbative regime. In Fig. 2(a), we show the E_{exc} -field dependence of I_{\parallel} and I_{\perp} for the 3rd and 5th HH. Here, θ is fixed at 22.5° so that finite I_{\perp} is allowed. In the low E_{exc} -field region, I_{\parallel} of the 3rd HH follows perturbative scaling, E_{exc}^6 , until 2.5 MV/cm, and it shows saturation behavior beyond that. However, as E_{exc} further increases, the saturation stops and I_{\parallel} increases at a rate even faster than E_{exc}^6 perturbative scaling. As a result, I_{\parallel} shows a kink structure in the intermediate E_{exc} -field region. Notably, above 3.5 MV/cm, I_{\parallel} of the 3rd HH follows a power law of E_{exc}^{10} , indicating that the 5th-order nonlinear process contributes to the 3rd HH emission (see also Supplemental Material [34]).

The anisotropy of the HH yields also indicates the involvement of a higher-order process. Figure 2(e) shows the θ dependence of the HH yields at different E_{exc} fields. The anisotropy of the 3rd HH yield shows a dramatic change when E_{exc} increases across the kink structure of the E_{exc} -field dependence around 3.5 MV/cm, with the most-efficient direction switching from $\theta = 0^\circ$ to $\theta = 45^\circ$. After the switch, the θ dependence of the 3rd HH yield coincides with that of the 5th HH.

On the other hand, I_{\perp} of the 3rd HH behaves totally differently from I_{\parallel} , as shown in Fig. 2(a). This fact reveals that I_{\parallel} and I_{\perp} are not expressible as simple projections of the single HH emission source in each direction, implying interplay of multiple emission sources. As a consequence of these different curves, $R_{\perp\parallel}$ grows nonmonotonically as E_{exc} increases, showing a peak around 3.5 MV/cm in Fig. 2(b).

This peculiar structure of $R_{\perp\parallel}$ is correlated to the HH polarization. Figure 2(f) shows the polarization of the HHs at $\theta = 22.5^\circ$ and at different E_{exc} fields. The polarization of the 3rd HH changes sharply around 3.5 MV/cm, with the major axis of polarization crossing $\phi = 0^\circ$. Importantly, the polarization state of the 3rd HH becomes elliptic around 3.5 MV/cm. We checked that the deviation from linear polarization is not due to the depolarization (see Supplemental Material [34]). The E_{exc} -field dependence of the major-axis angle and ellipticity are plotted in Figs. 2(c) and 2(d), which visualize the polarization switching and finite ellipticity appearing around the peak of $R_{\perp\parallel}$.

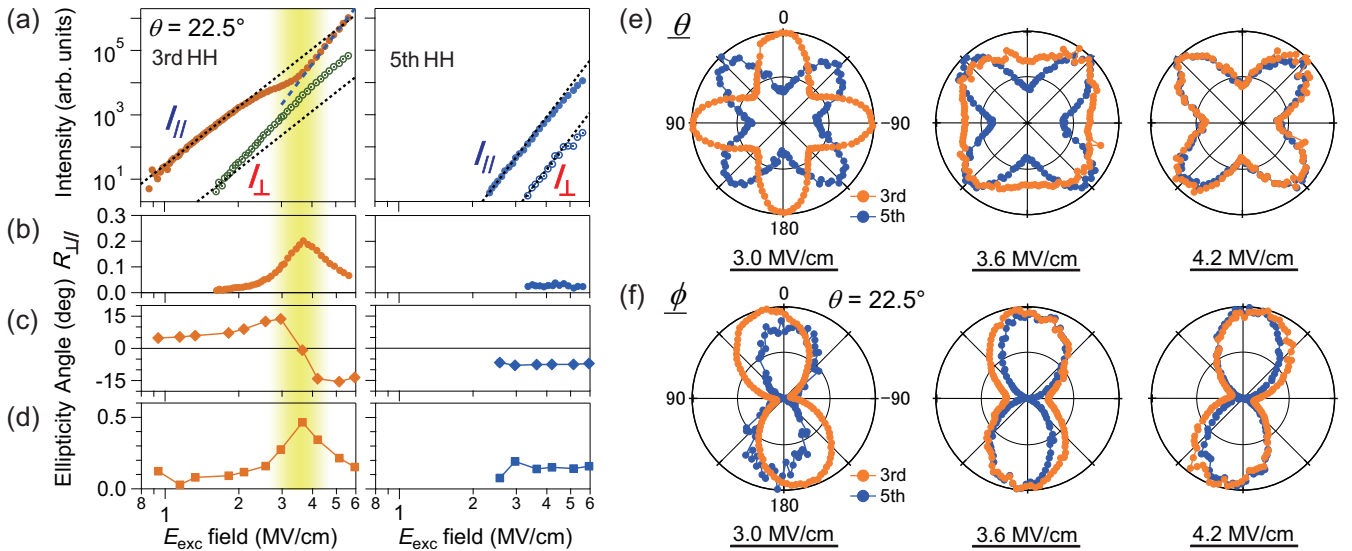


FIG. 2. (a)–(d) E_{exc} -field dependence of properties of 3rd and 5th HH generated by 0.83-eV excitation. (a) HH intensity I_{\parallel} and I_{\perp} . Black dotted lines indicate perturbative scaling for each order. The blue dashed line in the 3rd HH figure indicates 5th-order scaling. (b) Intensity ratio $R_{\perp\parallel} = I_{\perp}/I_{\parallel}$. (c) Major-axis angle of HH polarization relative to E_{exc} ($\phi = 0^\circ$). (d) HH ellipticity. (e), (f) (e) θ dependence of HH yields and (f) HH polarizations generated at $\theta = 22.5^\circ$ at three different E_{exc} fields.

Generation of elliptic HH and its E_{exc} -field dependence can be explained by the phase difference in nonlinear processes contributing to HHG as follows; the above-mentioned 3rd- and 5th-order nonlinear processes have different polarization directions and temporal emission phases. In the perturbative region, only the 3rd-order process contributes to the 3rd HH, and hence, the HH polarization is almost linear. With increasing E_{exc} , the contribution from the 5th-order nonlinear process grows in the guise of the 3rd HH [38]. When it becomes comparable to the original 3rd-order process, the two emission processes interfere to produce the elliptically polarized 3rd HH. In the even stronger E_{exc} region of extreme nonlinearity, the 5th-order nonlinear process dominates the emission and the interference becomes less substantial, resulting in the linear HH polarization. Taking this picture into account, the I_{\parallel} and I_{\perp} curves in Fig. 2(a) can be interpreted to be a consequence of interference of two emission processes with different nonlinearities, polarizations, and phases.

We should note that such an anomalous feature in the PEN crossover cannot be observed in the PL, which only reflects the density of photoinjected carriers. The E_{exc} -field dependence of the PL intensity shows a simple monotonic saturation (see Supplemental Material [34]). This stark contrast demonstrates that HHG provides a window through which one can observe complex coherent dynamics, that is difficult to even recognize using other methods.

The results obtained so far by using the 0.83-eV excitation revealed the emergence of a polarization anomaly in the 3rd HH in the PEN crossover region. However, in this case, the magnitude of $R_{\perp\parallel}$ remained modest ($\sim 20\%$ at the peak); hence, the degree of ellipticity remained modest. Then, a naive question arises: Does a larger anomaly occur in HHs of higher order?

In Fig. 2, the 5th HH stays within the perturbation regime in the whole region, showing no anomaly. However,

photoinduced damage to the sample prevented any investigation at stronger E_{exc} fields above 6.0 MV/cm. This experimental problem can be circumvented by using an excitation with a lower photon energy. In the following, we used 0.36-eV excitation pulses. This photoexcitation allowed us not only to apply a stronger E_{exc} , but also to observe higher-order HHs within our spectral window.

Figure 3 shows the E_{exc} -field dependence of the HH intensity and polarization state from the 5th to 11th order. θ was fixed to 22.5° . I_{\parallel} of the 5th HH shows a multikink structure after deviating from the perturbative scaling, which corresponds to the kink structure in Fig. 2(a). However, in contrast to the 0.83-eV excitation case, the switch of the major contribution to higher-order nonlinear processes cannot be clearly discerned in I_{\parallel} . Furthermore, the E_{exc} -field dependences of $R_{\perp\parallel}$, the major-axis angle, and ellipticity of HH polarization do not coincide perfectly, though they are loosely correlated. The obscure switching of nonlinearity order can be attributed to the longer excitation wavelength inducing a larger ponderomotive energy, which undermines the validity of the perturbative picture. Indeed, the Keldysh parameter γ [39,40], a criterion for the validity of the multiphoton perturbative picture, is smaller than 1 in the region $E_{\text{exc}} > 5.7$ MV/cm [34]. This particularly applies to higher-order HHG, for which a higher E_{exc} field is necessary.

Nevertheless, the anomaly in the HH polarization appears in a similar manner: namely, (1) I_{\parallel} and I_{\perp} show different curves resulting in a peak structure in $R_{\perp\parallel}$. $R_{\perp\parallel}$ increases above the perturbative region but starts to decrease after the peak, showing a small value at the high extreme of E_{exc} . For simplicity, we continue using the term ‘‘PEN crossover’’ to indicate this intermediate region where the peak of $R_{\perp\parallel}$ appears, although for higher-order HHs I_{\parallel} deviates from perturbation even at the lowest E_{exc} field. (2) Polarization shows an anomaly around the peak of $R_{\perp\parallel}$ for each HH. The

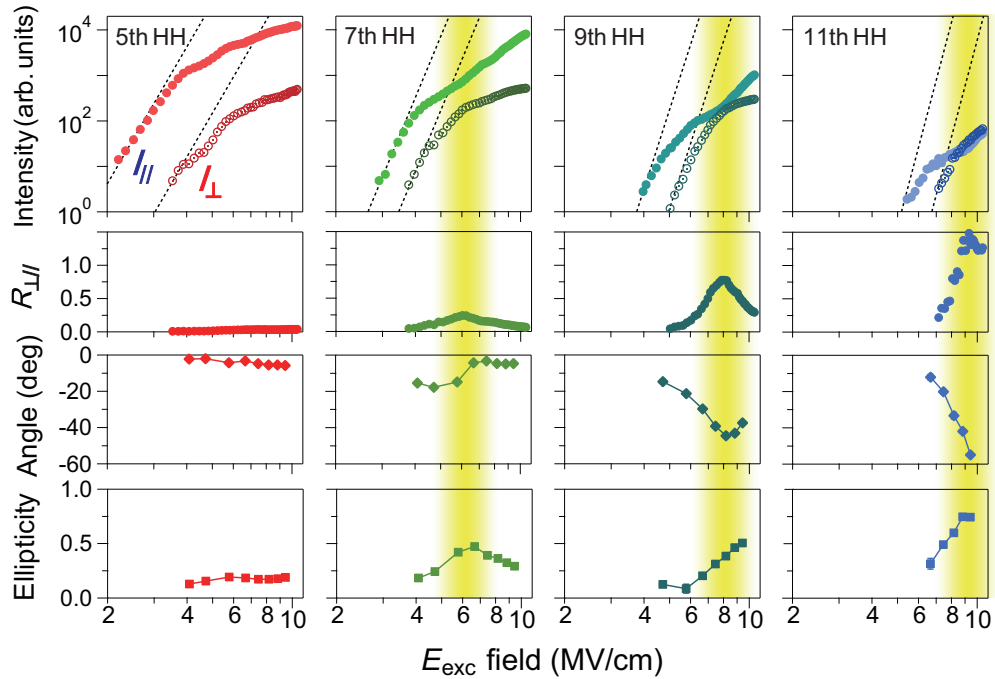


FIG. 3. E_{exc} -field dependence of I_{\parallel} , I_{\perp} , $R_{\perp\parallel} = I_{\perp}/I_{\parallel}$, major-axis angle, and ellipticity of polarization, of HHs generated by 0.36-eV excitations.

ellipticity being prominent in a limited region of the PEN crossover indicates that it is an outcome of the interference of different nonlinear emission processes. In Fig. 3, the polarization anomaly appears at a higher E_{exc} field for higher-order HH. This is because a higher E_{exc} field is necessary for realizing substantial contributions from higher-order nonlinear processes.

In Fig. 3, a higher peak value of $R_{\perp\parallel}$ appears for higher-order HH, exceeding 140% in the case of 11th order. This leads to exotic features of the HH polarization and anisotropy. Figure 4(a) shows the HH polarization of each order, measured at the E_{exc} field giving the peak in $R_{\perp\parallel}$ (a complete dataset can be found in [34]). Larger major-axis angle and ellipticity of the HH polarization are realized at higher orders. In particular, the 11th HH approaches a circularly polarized state (ellipticity up to 0.75). This result demonstrates that HH polarizations can be controlled by varying the E_{exc} -field strength. While continuous control of the nonlinear phase has previously been demonstrated utilizing metasurfaces [41,42]

or elliptically polarized excitation pulses [29,43], in this experiment, harmonic phase control was performed with a bulk crystal by tuning the power of linearly polarized excitation. Not only the polarization, but also the yield anisotropy shows anomalous features. Figure 4(b) plots the θ dependence of total HH yield ($I_{\parallel} + I_{\perp}$), together with I_{\parallel} and I_{\perp} , for each order (a complete dataset can be found in [34]). In general, I_{\parallel} takes a maximum at $\theta = 0^{\circ}$ or 45° . On the other hand, I_{\perp} is zero under such high symmetric conditions, and takes a maximum between them. Therefore, if $R_{\perp\parallel}$ is large, the total HH yield takes a maximum in a low symmetry direction such as $\theta = 22.5^{\circ}$, which is oriented along none of the bond directions. This exotic anisotropy demonstrates that the large OR in the PEN crossover affects significantly not only the polarization but also the total yield of the HH. Note that this large OR should be distinguished from the perpendicularly but linearly polarized *even-order* HHG in materials with broken inversion symmetry, originating from the Berry-curvature-induced intraband current [25,26].

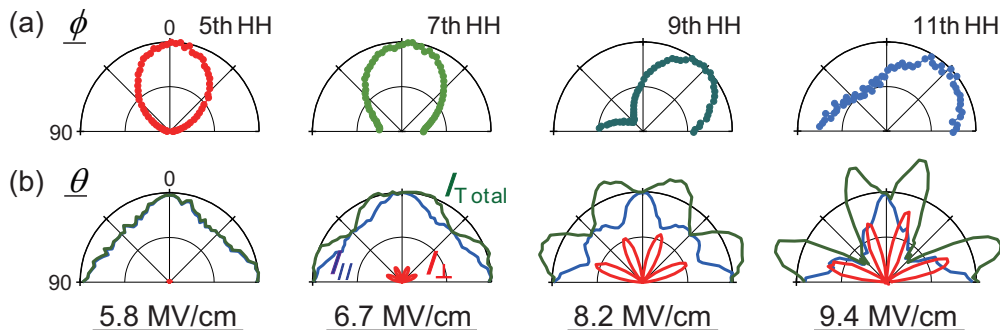


FIG. 4. (a) Polarization state generated at $\theta = 22.5^{\circ}$ and (b) θ dependence of the HH yield shown with I_{\parallel} and I_{\perp} . For each order HH, E_{exc} was set so that $R_{\perp\parallel}$ is at a maximum for each order HH.

IV. DISCUSSION

Now let us discuss the important factors for achieving a large $R_{\perp\parallel}$, and in turn a large HH ellipticity. As already explained, photoinduced nonlinear dynamics is necessary to obtain a finite OR in GaAs. This is because the contributions from k points in the Brillouin zone are averaged on the isoenergy plane, causing cancellation of OR in cubic semiconductors in the linear-response regime, whereas a finite OR survives in the nonlinear regime when E_{exc} is applied in a low symmetry direction. Furthermore, nonlinear dynamics needs to host multiple emission channels with comparable amplitudes and different phases, which is possible around the PEN crossover.

Besides the nonlinear dynamics, the energy of the HH emission is also crucial. Notably, in the 5th HHG by 0.36-eV excitations, $R_{\perp\parallel}$ is limited to a tiny value in the whole E_{exc} region, leading to negligible polarization anomaly. This behavior should be compared with that of the 3rd HHG by 0.83-eV excitations, which has a smaller HH order but shows larger $R_{\perp\parallel}$ and polarization anomaly. Thus, the small $R_{\perp\parallel}$ value of the 5th HH by 0.36-eV excitations can be ascribed to its emission energy, which lies close to the band gap of 1.42 eV. In this experiment, all HHs had photon energies above the band gap, indicating that the HH emissions were mainly caused by the interband currents [13,19,20]. The band dispersions in GaAs are almost isotropic near the band edge at the Γ point; hence, recombination in this region cannot produce a large polarization perpendicular to E_{exc} , even factoring in the nonlinear dynamics. In contrast, the peak $R_{\perp\parallel}$ value continuously increases for higher-order HHs emitted at higher energies, as shown in Fig. 3. This can be explained by the band structure becoming anisotropic for k points away from the band edge, with a winding energy landscape, giving a chance for a large polarization perpendicular to E_{exc} [23,28,44]. In addition, for larger k points, energy splitting of the valence bands, i.e., light-hole, heavy-hole, and the split-off band, becomes larger

[45]. This band split causes the recombination for the same HH emission energy at different k points depending on the valence bands, which results in multiple emission channels with different dipole moments and phases that are ingredients for the elliptic HHG. Therefore, the large HH ellipticity in GaAs is generated by the nonlinear dynamics in the PEN crossover under the condition that the emission processes occur away from the band edge. Taking the above discussion into account, the polarization anomaly will provide an alternative probe to investigate band characteristics far away from the band edge.

V. SUMMARY

In conclusion, we investigated the HH polarization generated from GaAs across the PEN crossover. With a linearly polarized E_{exc} in the low symmetry crystal direction, nonlinear OR induces perpendicularly polarized HH components. These perpendicular components become prominent in the PEN crossover, inducing an anomaly in the HH polarization and yield anisotropy. In particular, the emergent ellipticity of HHs indicates the contribution of multiple emission processes with different nonlinearities and temporal phases. These results demonstrate that the HH polarization provides a sensitive probe for the dramatic changes in the coherent nonlinear dynamics across the PEN crossover. An intriguing question for the future is how material properties such as the band gaps, dispersions, degeneracies, and Berry curvatures affect the HH polarization anomaly. Further study of the microscopic mechanisms relevant to the HH polarization anomaly will provide us with a compass to find a material for a polarization- and wavelength-tunable ultrafast light source.

ACKNOWLEDGMENTS

We thank Y. Sanari for technical support, and S. A. Sato for fruitful discussions. Part of this study was supported by JSPS KAKENHI Grant No. JP19H05465.

-
- [1] See, e.g., M. Born and E. Wolf, *Principles of Optics: Electromagnetic Theory of Propagation, Interference and Diffraction of Light* (Elsevier, New York, 2013).
 - [2] I. Sodemann and L. Fu, *Phys. Rev. Lett.* **115**, 216806 (2015).
 - [3] Q. Ma, S.-Y. Xu, H. Shen, D. MacNeill, V. Fatemi, T.-R. Chang, A. M. Mier Valdivia, S. Wu, Z. Du, C.-H. Hsu, S. Fang, Q. D. Gibson, K. Watanabe, T. Taniguchi, R. J. Cava, E. Kaxiras, H.-Z. Lu, H. Lin, L. Fu, N. Gedik, and P. Jarillo-Herrero, *Nature (London)* **565**, 337 (2019).
 - [4] J. B. Costello, S. D. O'Hara, Q. Wu, D. C. Valocin, L. N. Pfeiffer, K. W. West, and M. S. Sherwin, *Nature (London)* **599**, 57 (2021).
 - [5] A. Sell, A. Leitenstorfer, and R. Huber, *Opt. Lett.* **33**, 2767 (2008).
 - [6] H. Hirori, A. Doi, F. Blanchard, and K. Tanaka, *Appl. Phys. Lett.* **98**, 91106 (2011).
 - [7] G. Andriukaitis, T. Balčiūnas, S. Ališauskas, A. Pugžlys, A. Baltuška, T. Popmintchev, M.-C. Chen, M. M. Murnane, and H. C. Kapteyn, *Opt. Lett.* **36**, 2755 (2011).
 - [8] N. Kanda, N. Ishii, J. Itatani, and R. Matsunaga, *Opt. Express* **29**, 3479 (2021).
 - [9] Y. Sanari, F. Sekiguchi, K. Nakagawa, N. Ishii, Y. Kanemitsu, and H. Hirori, *Opt. Lett.* **46**, 5280 (2021).
 - [10] A. H. Chin, O. G. Calderón, and J. Kono, *Phys. Rev. Lett.* **86**, 3292 (2001).
 - [11] S. Ghimire, A. D. DiChiara, E. Sistrunk, P. Agostini, L. F. DiMauro, and D. A. Reis, *Nat. Phys.* **7**, 138 (2011).
 - [12] D. Golde, T. Meier, and S. W. Koch, *Phys. Rev. B* **77**, 075330 (2008).
 - [13] G. Vampa, C. R. McDonald, G. Orlando, D. D. Klug, P. B. Corkum, and T. Brabec, *Phys. Rev. Lett.* **113**, 073901 (2014).
 - [14] O. Schubert, M. Hohenleutner, F. Langer, B. Urbanek, C. Lange, U. Huttner, D. Golde, T. Meier, M. Kira, S. W. Koch, and R. Huber, *Nat. Photonics* **8**, 119 (2014).
 - [15] Y. S. You, D. A. Reis, and S. Ghimire, *Nat. Phys.* **13**, 345 (2017).
 - [16] F. Langer, M. Hohenleutner, U. Huttner, S. W. Koch, M. Kira, and R. Huber, *Nat. Photonics* **11**, 227 (2017).

- [17] T. T. Luu, M. Garg, S. Y. Kruchinin, A. Moulet, M. T. Hassan, and E. Goulielmakis, *Nature (London)* **521**, 498 (2015).
- [18] G. Vampa, T. J. Hammond, N. Thiré, B. E. Schmidt, F. Légaré, C. R. McDonald, T. Brabec, D. D. Klug, and P. B. Corkum, *Phys. Rev. Lett.* **115**, 193603 (2015).
- [19] A. J. Uzan, G. Orenstein, Á. Jiménez-Galán, C. McDonald, R. E. F. Silva, B. D. Bruner, N. D. Klimkin, V. Blanchet, T. Arusi-Parpar, M. Krüger, A. N. Rubtsov, O. Smirnova, M. Ivanov, B. Yan, T. Brabec, and N. Dudovich, *Nat. Photonics* **14**, 183 (2020).
- [20] N. Yoshikawa, K. Nagai, K. Uchida, Y. Takaguchi, S. Sasaki, Y. Miyata, and K. Tanaka, *Nat. Commun.* **10**, 3709 (2019).
- [21] Y. Sanari, T. Otobe, Y. Kanemitsu, and H. Hirori, *Nat. Commun.* **11**, 3069 (2020).
- [22] S. Jiang, J. Chen, H. Wei, C. Yu, R. Lu, and C. D. Lin, *Phys. Rev. Lett.* **120**, 253201 (2018).
- [23] K. Uchida, V. Pareek, K. Nagai, K. M. Dani, and K. Tanaka, *Phys. Rev. B* **103**, L161406 (2021).
- [24] H. Lakhotia, H. Y. Kim, M. Zhan, S. Hu, S. Meng, and E. Goulielmakis, *Nature (London)* **583**, 55 (2020).
- [25] H. Liu, Y. Li, Y. S. You, S. Ghimire, T. F. Heinz, and D. A. Reis, *Nat. Phys.* **13**, 262 (2017).
- [26] T. T. Luu and H. J. Wörner, *Nat. Commun.* **9**, 916 (2018).
- [27] C. P. Schmid, L. Weigl, P. Grössing, V. Junk, C. Gorini, S. Schlauderer, S. Ito, M. Meierhofer, N. Hofmann, D. Afanasiev, J. Crewse, K. A. Kokh, O. E. Tereshchenko, J. Gütde, F. Evers, J. Wilhelm, K. Richter, U. Höfer, and R. Huber, *Nature (London)* **593**, 385 (2021).
- [28] K. Kaneshima, Y. Shinohara, K. Takeuchi, N. Ishii, K. Imasaka, T. Kaji, S. Ashihara, K. L. Ishikawa, and J. Itatani, *Phys. Rev. Lett.* **120**, 243903 (2018).
- [29] N. Klemke, N. Tancogne-Dejean, G. M. Rossi, Y. Yang, F. Scheiba, R. E. Mainz, G. Di Sciacca, A. Rubio, F. X. Kärtner, and O. D. Mücke, *Nat. Commun.* **10**, 1319 (2019).
- [30] G. Ndabashimiye, S. Ghimire, M. Wu, D. A. Browne, K. J. Schafer, M. B. Gaarde, and D. A. Reis, *Nature (London)* **534**, 520 (2016).
- [31] Y. Murakami, M. Eckstein, and P. Werner, *Phys. Rev. Lett.* **121**, 057405 (2018).
- [32] P. Xia, T. Tamaya, C. Kim, F. Lu, T. Kanai, N. Ishii, J. Itatani, H. Akiyama, and T. Kato, *Phys. Rev. B* **104**, L121202 (2021).
- [33] T.-Y. Du, D. Tang, and X.-B. Bian, *Phys. Rev. A* **98**, 063416 (2018).
- [34] See Supplemental Material at <http://link.aps.org/supplemental/10.1103/PhysRevB.106.L241201> for the details of experimental setup; reflection in the linear-response regime; zoomed-in version of Fig. 2(a); confirmation of the elliptical polarization of the HH; anisotropy and excitation-field dependence of the PL; detailed argument on the symmetry and HH polarizations; evaluation of the Keldysh parameter; and complete datasets of the polarization and anisotropy of HHs generated by the 0.36-eV excitations; also see Refs. [9,39,40].
- [35] J. E. Sipe, D. J. Moss, and H. M. van Driel, *Phys. Rev. B* **35**, 1129 (1987).
- [36] D. C. Hutchings and B. S. Wherrett, *Phys. Rev. B* **49**, 2418 (1994).
- [37] Y. Sanari, H. Hirori, T. Aharen, H. Tahara, Y. Shinohara, K. L. Ishikawa, T. Otobe, P. Xia, N. Ishii, J. Itatani, S. A. Sato, and Y. Kanemitsu, *Phys. Rev. B* **102**, 041125(R) (2020).
- [38] T. Tritschler, O. D. Mücke, M. Wegener, U. Morgner, and F. X. Kärtner, *Phys. Rev. Lett.* **90**, 217404 (2003).
- [39] L. V. Keldysh, *Sov. Phys. JETP* **20**, 1307 (1965).
- [40] C. Lange, T. Maag, M. Hohenleutner, S. Baierl, O. Schubert, E. R. J. Edwards, D. Bougeard, G. Woltersdorf, and R. Huber, *Phys. Rev. Lett.* **113**, 227401 (2014).
- [41] G. Li, S. Chen, N. Pholchai, B. Reineke, P. W. H. Wong, E. Y. B. Pun, K. W. Cheah, T. Zentgraf, and S. Zhang, *Nat. Mater.* **14**, 607 (2015).
- [42] S. D. Gennaro, M. Rahmani, V. Giannini, H. Aouani, T. P. H. Sidiropoulos, M. Navarro-Cía, S. A. Maier, and R. F. Oulton, *Nano Lett.* **16**, 5278 (2016).
- [43] N. Tancogne-Dejean, O. D. Mücke, F. X. Kärtner, and A. Rubio, *Nat. Commun.* **8**, 745 (2017).
- [44] H. B. Banks, Q. Wu, D. C. Valocin, S. Mack, A. C. Gossard, L. Pfeiffer, R.-B. Liu, and M. S. Sherwin, *Phys. Rev. X* **7**, 041042 (2017).
- [45] J. R. Chelikowsky and M. L. Cohen, *Phys. Rev. B* **14**, 556 (1976).